





RESEARCH ARTICLE

Modulation effect of substantia nigra iron deposition and functional connectivity on putamen glucose metabolism in Parkinson's disease

Zhenxiang Zang^{1,2}  | Tianbin Song^{1,2} | Jiping Li³ | Shaozhen Yan^{1,2}  |
Binbin Nie⁴ | Shanshan Mei⁵ | Jie Ma^{1,2} | Yu Yang^{1,2} | Baoci Shan⁴  |
Yuqing Zhang³ | Jie Lu^{1,2} 

¹Department of Radiology and Nuclear Medicine, Xuanwu Hospital, Capital Medical University, Beijing, China

²Beijing Key Laboratory of Magnetic Resonance Imaging and Brain Informatics, Beijing, China

³Beijing Institute of Functional Neurosurgery, Xuanwu Hospital, Capital Medical University, Beijing, China

⁴Beijing Engineering Research Center of Radiographic Techniques and Equipment, Institute of High Energy Physics, Chinese Academy of Sciences, China

⁵Department of Neurology, Xuanwu Hospital, Capital Medical University, Beijing, China

Correspondence

Jie Lu, Department of Radiology and Nuclear Medicine, Xuanwu Hospital, Capital Medical University, Changchun Road, No. 45, Beijing 100053, China.
Email: imaginglu@hotmail.com

Funding information

Beijing Municipal Administration of Hospitals' Ascent Plan, Grant/Award Number: DFL20180802; Huizhi Ascent Project of Xuanwu Hospital, Grant/Award Number: HZ2021ZCLJ005

Abstract

Neurodegeneration of the substantia nigra affects putamen activity in Parkinson's disease (PD), yet in vivo evidence of how the substantia nigra modulates putamen glucose metabolism in humans is missing. We aimed to investigate how substantia nigra modulates the putamen glucose metabolism using a cross-sectional design. Resting-state fMRI, susceptibility-weighted imaging, and [¹⁸F]-fluorodeoxyglucose-PET (FDG-PET) data were acquired. Forty-two PD patients and 25 healthy controls (HCs) were recruited for simultaneous PET/MRI scanning. The main measurements of the current study were R_2^* images representing iron deposition (28 PD and 25 HCs), standardized uptake value ratio (SUVr) images representing FDG-uptake (33 PD and 25 HCs), and resting state functional connectivity maps from resting state fMRI (34 PD and 25 HCs). An interaction term based on the general linear model was used to investigate the joint modulation effect of nigral iron deposition and nigral-putamen functional connectivity on putamen FDG-uptake. Compared with HCs, we found increased iron deposition in the substantia nigra ($p = .007$), increased FDG-uptake in the putamen (left: $P_{FWE} < 0.001$; right: $P_{FWE} < 0.001$), and decreased functional connectivity between the substantia nigra and the anterior putamen (left $P_{FWE} < 0.001$, right: $P_{FWE} = 0.007$). We then identified significant interaction effect of nigral iron deposition and nigral-putamen connectivity on FDG-uptake in the putamen ($p = .004$). The current study demonstrated joint modulation effect of the substantia nigra iron deposition and nigral-putamen functional connectivity on putamen glucose metabolic distribution, thereby revealing in vivo pathological mechanism of nigrostriatal neurodegeneration of PD.

KEYWORDS

nigral iron deposition, nigrostriatal functional connectivity, Parkinson's disease, putamen metabolism distribution

1 | INTRODUCTION

Parkinson's disease (PD) is the second most common neurodegenerative disease after Alzheimer's disease, which manifests clinical features such as resting tremor, bradykinesia, or rigidity (Maiti et al., 2017). Over the past decades, a variety of animal as well as post-mortem studies have established pathological models of PD in which the neurodegeneration of the substantia nigra as well as the nigrostriatal pathway (Dauer & Przedborski, 2003) are characterized as the hallmark features (Iravani et al., 2005; Porras et al., 2012).

Dopaminergic cell loss as well as iron deposition in the substantia nigra are consistently described as the neurodegeneration hallmark of PD (Dauer & Przedborski, 2003). Excessive iron deposition was a potential cause of dopaminergic neuron loss in the substantia nigra pars compacta (Langley et al., 2019) due to iron accumulation induced α -synuclein aggregation which could cause the increases of toxicity effect and downregulation of the dopamine marker (Chu et al., 2019; Ostrerova-Golts et al., 2000; Ward et al., 2014). Observations from various studies have pointed toward increased nigral iron load in patients with PD (Graham et al., 2000; Guan et al., 2019; Zhang et al., 2010). Therefore, iron deposition in the substantia nigra has been characterized as a phenotype that is closely associated with nigral neurodegeneration.

Abnormal glucose metabolism in the striatum has been consistently reported in PD as revealed by ^{18}F -FDG PET imaging in the past decades (Albrecht et al., 2019; Meyer et al., 2017; Ruppert et al., 2020; Schindlbeck & Eidelberg, 2018). An early study by Wooten and Collins had shown that lesion in the substantia nigra can induce disinhibition to the striatum in a rat model (Wooten & Collins, 1981). Neurodegeneration of the substantia nigra could cause abnormal activity in the striatal loop and further contributes to PD's core symptoms (DeLong, 1990; McGregor & Nelson, 2019). Indicatively therefore, as a hallmark of neurodegeneration in the substantia nigra, excessive iron deposition may lead to impaired activity in the striatum. However, clarification of *in vivo* evidence linking substantia nigra iron deposition to striatal metabolism in PD is still pending.

The striatum receives dopaminergic input from the substantia nigra via the nigrostriatal pathway. In rodent models, applications of 6-hydroxydopamine (6-OHDA) on the nigrostriatal pathway could lead to nigral dopaminergic cell loss as well as striatal fiber degeneration (Jeon et al., 1995; Rentsch et al., 2019). Resting-state functional magnetic resonance imaging (RS-fMRI) provides a noninvasive approach for *in vivo* estimation of the functional nigrostriatal pathway. Functional connectivity (FC) study by Hacker and colleagues identified decreased FC between the putamen and midbrain regions including the substantia nigra (Hacker et al., 2012). A comparable result was later presented in another RS-fMRI study (Manza et al., 2016) where decreased FC between the anterior putamen and the substantia nigra was correlated with more severe behavioral impairment, demonstrating that the reduced connectivity between the putamen and the substantia nigra is reproducible *in vivo* feature representing the impaired nigrostriatal pathway.

Collectively, increased iron deposition and glucose metabolism may characterize the neurodegeneration feature of the substantia nigra and the abnormal activity of the putamen respectively. Decreased FC was also detected as a representation of impairment of the nigrostriatal pathway. Questions regarding whether the nigral iron deposition can independently influence the putamen metabolism or it modulates the putamen metabolism jointly with nigro-putamen FC are critical for revealing the pathological mechanisms of the nigrostriatal loop of PD.

PET/MRI scanner acquires functional and metabolic data simultaneously, which is critical for capturing the dynamically-changing brain activities. Therefore, we acquired simultaneous ^{18}F -fluorodeoxyglucose (FDG) PET/fMRI as well as susceptibility-weighted imaging data during resting state. Two aims were addressed: first, based on previous neuroimaging findings (Guan et al., 2019; Hacker et al., 2012; Schindlbeck & Eidelberg, 2018), we intended to replicate increased iron deposition in the substantia nigra and increased FDG-uptake in the putamen as well as a decreased FC between the substantia nigra and the putamen in group comparisons. Second, we aimed to investigate how nigral iron deposition and nigrostriatal FC modulate putamen glucose metabolism.

2 | MATERIALS AND METHODS

2.1 | Participants

All participants provided written informed consent before the measurement. The current study was approved by the ethics committee of Xuanwu Hospital.

Cross-sectional data were collected at Xuanwu Hospital, Capital Medical University in the year 2019 and 2020. We recruited PD patients according to the following criteria: (1) All patients were diagnosed with MDS-PD criteria (Postuma et al., 2015, 2018); (2) age between 40–75 years old; (3) right-handed; (4) no history of head trauma, cerebral vascular disease, and psychiatric disease; (5) no current alcohol or drug abuse. In total, 42 PD patients were recruited for RS-fMRI scan, SWI-plus scan and simultaneous ^{18}F -FDG PET scan from the department of functional neurosurgery. We further excluded participants according to: (1) over 30% time points that exceeded 0.5 mm frame-wise displacement during RS-fMRI scan and (2) incidental findings of visible brain impairment. As a result, we excluded eight PD subjects with large head motion during RS-fMRI scan, leaving 34 PD patients and 25 age and sex-matched healthy controls (HC) for further analyses. The right-handed HCs (1) reported no history of substance drug abuse, traumatic brain injury, cerebrovascular events, neuroinflammation, neurological and psychiatric conditions and (2) did show signs of movement problem and cognitive impairment during the interview with the neurologists. PD patients were instructed to not use dopaminergic medication for at least 12 h prior to the scan. The detailed information of all participants was provided in Table 1.

TABLE 1 Demographic information of subjects

	Healthy controls	Parkinson's disease	p-Value	Test statistics
Number	25	34 (42 recruited)		
Sex (m/f)	8/17	13/21	.62	$\chi^2 = 0.24$
Age (\pm SD)	60.00 \pm 4.54	62.32 \pm 6.40	.13	$T = -1.55$
FD power (\pm SD)	0.22 \pm 0.09	0.21 \pm 0.08	.60	$T = 0.53$
HY-stage (\pm SD)		3.00 \pm 0.83		
UPDRSIII (\pm SD)		59.71 \pm 15.00		
Disease duration (\pm SD)		9.59 \pm 4.04		

Note: Mean \pm standard deviations are shown.

Abbreviations: FD, frame-wise displacement; HY-stage, Hoehn and Yahr stage; UPDRSIII, Unified Parkinson's Disease Rating Scale—III.

2.2 | Hybrid PET/MR data acquisition

All subjects underwent hybrid PET/MR examination (averaged duration between tracer injection and scan was 1 h) by using hybrid PET/MR system (uPMR790, UIH), which features simultaneous PET imaging with 3.0 T MR with a 24-channel head/neck coil. All patients were fasted for at least 6 h before PET/MR examination. The injected dose of ^{18}F -FDG of subject was 3.7 MBq/kg. PET acquisition time of one bed position lasted 10 min covering from the top of the skull. PET data were reconstructed with TOF technology. The reconstruction parameters were: 4 iterations, 20 subsets, Gaussian filter is 3 mm, matrix size is 256×256 , thickness is 2.8 mm. Field of view (FOV): $300 \text{ mm} \times 300 \text{ mm}$, voxel size: $2.4 \text{ mm} \times 2.4 \text{ mm} \times 2.8 \text{ mm}$.

Resting-state fMRI was acquired using an echo-planar imaging (EPI) sequence with the following parameters: TR = 2000 ms, TE = 30 ms, slice thickness = 3.5 mm, voxel size = $3.5 \times 3.5 \times 3.5 \text{ mm}^3$, 0.7 mm slice gap, 31 slices, $230 \times 230 \text{ mm}$ FOV, and 90° flip angle. Before resting-state data acquisition, we instructed participants to close their eyes, relax, and not engage in any particular mental activity during the scan (230 volumes). After each scan, the participants reported that they did not fall asleep in the scanner. In addition, we acquired high-resolution three-dimensional T1-weighted images with the following parameters: TR = 7.9 ms, TE = 3.8 ms, 176 slices, FOV = $256 \times 256 \text{ mm}$, and 1 mm^3 spatial resolution.

A three-dimensional (3D) multi-echo gradient-echo (GRE) sequence was used for SWI-plus data acquisition with the following parameters: FA = 15° , voxel size = $1 \times 1 \times 2 \text{ mm}^3$ (interpreted as 1 mm^3), repetition time = 29 ms, six echo times = 3.1/6.4/9.7/13.0/16.3/19.6 ms, and bandwidth = 500 Hz/px, acquisition matrix: 256×256 , number of slices: 68, slice orientation: F-H, parallel imaging, acceleration factor: 2, and monopolar readout gradients were used with a total scan time of 5 min and 41 s.

2.3 | R_2^* image calculation and processing

Among all 59 subjects (25 HC and 34 PD), we acquired and analyzed SWI-plus images for 53 subjects (SWI-plus images from six patients with PD were failed for image reconstruction, leaving 25 HC and

28 PD). After image acquisition, the raw images were processed using the package implemented on the scanner system. In detail, a complex multi-dimensional integration (MDI) approach was adopted to achieve R_2^* calculation (Ye et al., 2021). In the MDI framework, R_2^* is extracted as the amount of signal relaxation ΔS during the echo spacing interval, which can be written for each channel as:

$$\Delta S(n_c) \equiv \frac{S(n_{e+1}, n_c)}{S(n_e, n_c)} = e^{-\frac{\Delta TE}{T_2^*} + i\Delta\omega\Delta TE}, \quad (1)$$

where S is the complex image signal of the corresponding echo and channel, ΔTE is the echo spacing, $\Delta\omega$ is the total off-resonant effects, and n_c represents each channel. MDI yields the numerical solution of ΔS , that is, $\Delta S'$, by solving the following optimization problem:

$$\min_{\Delta S'} \sum_{ne=1}^{Ne-1} \sum_{nc=1}^{Nc} \|S_{ne+1,nc} - S_{ne,nc} \cdot \Delta S'\|_2^2, \quad (2)$$

where Nc is the total number of coil channels. Then R_2^* value can be determined as:

$$R_2^* = -\frac{\ln|\Delta S'|}{\Delta TE}. \quad (3)$$

Finally, the R_2^* images were normalized to standard MNI space. R_2^* values were extracted from the bilateral substantia nigra for further analyses.

2.4 | PET images processing

PET images were processed in Statistical Parametric Mapping software (SPM12, <http://www.fil.ion.ucl.ac.uk/spm/software/spm12/>). PET images were firstly coregistered to T1 images and then spatially normalized to standard MNI coordinates. An 8-mm full width at half maximum (FWHM) Gaussian kernel was used for spatial smoothing.

For SUVr calculation, we applied an iterative data-driven approach for the identification of reference region to account for global confounds (Nie et al., 2018). At first, (1) Whole brain was selected as the initial reference region, named Ref0; (2) Voxel-wised two-sample t test was performed between the preprocessed images of PD patients and HC, using the mean value of Ref0 to account for global confounds; (3) Then, the

significant regions in PD patients are yielded based at a threshold of $p < .05$ (uncorrected), named SigRegion; (4) Excluding SigRegion from Ref0, and these remained voxels were selected as the new reference region, named Ref1; (5) Chose Ref1 as the new Ref0, and repeat the steps 2–5 until the residual deviation between the Ref1 and Ref0 was reduced by less than 5%; (6) The latest Ref1 was accepted as the data-driven unbiased reference region.

One patient was excluded due to enormous imaging artifact, resulting in 58 subjects in total for further PET-related analyses (25 HC, 33 PD).

2.5 | fMRI data processing

Image processing was performed using the SPM12. All images were realigned for head motion correction, slice timing, coregistered to the high-resolution 3D T1 images, segmentation of six tissue possibility templates (SPM12), and normalization of functional images via T1 images (resampled to $3 \times 3 \times 3 \text{ mm}^3$). The normalized functional images were then spatially smoothed with an 8-mm FWHM Gaussian kernel. After spatial smoothing, we further regressed out the time series of white matter (WM 99% probability SPM map), cerebrospinal fluid (CSF 90% probability SPM map) (Zang et al., 2018), global mean time course, six head motion parameters from the realignment step, and the frame-wise displacement (FD) (Power et al., 2012). As mentioned above, we excluded subjects with over 30% time points that exceeded 0.5-mm FD. Eight PD subjects were excluded, leaving 34 PD patients and 25 HC for fMRI analyses.

2.6 | Substantia nigra seed selection and coherence calculation

After image processing, the substantia nigra was selected based on a previously defined atlas (Pauli et al., 2018). In detail, we merged the bilateral substantia nigra as well as the substantia nigra pars reticulata and compacta together in order to generate a relatively large ROI for further analyses (Figure S1). Coherence was calculated based on MATLAB “mscohere.m” function which generates power spectrum coherence outputs for 129 frequency bins from 0 to 0.25 Hz as described in previous study (Salami et al., 2018). We used coherence not only because it has been widely applied in fMRI studies (Bassett et al., 2015; Braun et al., 2016), but also due to the reason that it estimates the signal synchronicity in the frequency domain, which is not influenced by signal phase difference. We then averaged the coherence outputs between 0.01 and 0.1 Hz band and considered the averaged coherence as the FC between the bilateral substantia nigra and other voxels. Since we had a prior hypothesis of the nigral-putamen loop, we therefore only focus on the voxels within the putamen (i.e. overlap with AAL's putamen mask).

Substantia nigra grey matter volume calculation.

To calculate the grey matter volume of the substantia nigra, we applied a voxel-based morphometry toolbox (VBM8, [http://dbm.neuro.](http://dbm.neuro.uni-jena.de/vbm8/)

[uni-jena.de/vbm8/](http://dbm.neuro.uni-jena.de/vbm8/)) using default parameters. The preprocessing was performed as described in a previous study (Zang et al., 2018). Briefly, brain tissue was classified and normalized to MNI space with a diffeomorphic image registration algorithm, correction for image intensity non-uniformity, a thorough cleaning up of gray matter partitions, application of a hidden Markov random field model, transformation of grey matter density values into volume equivalents, and smoothing with an 8-mm FWHM Gaussian kernel. Averaged grey matter volume was extracted from the pre-defined substantia nigra ROI.

2.7 | Group-level analyses

Comparisons of the FC and ^{18}F -FDG uptake (standardized uptake value ratio, SUVr) between HC and PD were conducted using two-sample t test from the SPM General Linear Model (GLM). We only focus on the voxels in bilateral putamen (AAL mask) according to our hypothesis. Since age was not perfectly balanced ($p = .13$), we controlled age as covariate of non-interest for group comparisons. In addition, averaged FD was controlled as covariate of non-interest for FC group analysis to further constrain the influence of head motion. Clusters with voxels surviving family-wise error (FWE) within the putamen were considered as significant (small volume correction). Comparisons were only performed within the AAL-putamen mask.

Comparisons of the grey matter volume, iron deposition as well as the ^{18}F -FDG uptake in the substantia nigra were done using the mean values of each imaging modality from the pre-defined ROI. Since the grey matter volume and iron deposition may influence each other (Lee et al., 2013), we controlled the substantia nigra grey matter volume (SN-GMV) as a covariate of non-interest for iron deposition analyses.

Post hoc comparisons and correlation analyses were done using SPSS26 (<https://www.ibm.com/analytics/spss-statistics-software>) software. Results with $p < .05$ were considered significant. In order to increase the sample size in the correlation analyses, we combined both HC and PD groups and controlled group as covariate of non-interests.

Since the nigrostriatal FC may be a critical factor in modulating glucose metabolism in the putamen, we next aimed to investigate the joint effect of nigral iron deposition and nigral-putamen FC on putamen FDG SUVr. We introduced an interaction term into the GLM as shown:

$$FDG_{(PUT)} = Iron_{(SN)} + FC_{(SN-PUT)} + Iron_{(SN)} \times FC_{(SN-PUT)} + Covariates. \quad (4)$$

In this model, we were interested in the $Iron_{(SN)} \times FC_{(SN-PUT)}$ interaction term while controlling for group and SN-GMV as covariates of non-interests. PUT_{FDG} refers to the SUVr values extracted from the putamen. $FC_{(SN-PUT)}$ refers to the FC between the substantia nigra and the putamen and $Iron_{(SN)}$ refers to iron deposition in the substantia nigra. We extracted the mean SUVr and FC values from the voxels that were considered significant in the putamen (voxels with $P_{FWE} < 0.05$) for this analysis. Group and SN-GMV were controlled as covariates of non-interests.

3 | RESULTS

3.1 | Clinical and demographic data

The clinical and demographic data are summarized in Table 1. Thirty-four PD patients and 25 age ($p = .13$) and sex ($p = .62$) matched HC were used for fMRI analysis. Fifty-three subjects (28 PD and 25 HC, SWI-plus images from six PD were failed for image reconstruction) were analyzed for R_2^* and 58 subjects (33 PD and 25 HC, PET image from one PD were excluded due to huge image noise) were analyzed for PET. Joint analyses of all imaging modalities were carried out based on 53 subjects (28 PD and 25HC). The number of subjects available for all analyses were provided in Table S1.

3.2 | Grey matter atrophy in the substantia nigra

Compared with the HC group, we found a significantly decreased grey matter volume of the substantia nigra while controlling for age and total intracranial volume (TIV) as covariate of non-interests ($T_{[55]} = -2.79$, $p = .007$). There was a trend-to-significance correlation between SN-GMV and iron deposition ($R = -0.24$, $p = .09$). Therefore, controlling for SN-GMV as covariate of non-interest in the analyses associated with iron deposition was necessary. No significant correlations were found between the SN-GMV and the HY-stage, UPDRS III score, and the disease duration (p values $>.09$).

3.3 | Increased iron deposition in the substantia nigra

We compared the averaged R_2^* values from the bilateral substantia nigra ROI and found a significant increase of iron deposition in the PD group compared with the HC group ($T_{[49]} = 2.81$, $p = .007$, $\eta^2 = 0.14$,

age and SN-GMV as covariates of non-interests, Figure 1a,b). Note that Figure 1a was a display of voxel-wise R_2^* comparison to show the spatial distribution of the voxels with increased iron deposition in PD. Post hoc statistical analyses and inference were all based on the results shown in Figure 2b. The R_2^* value of the substantia nigra significantly positively correlate with the HY-stage ($R = 0.43$, $p = .023$, $\eta^2 = 0.18$) and the disease duration ($R = 0.49$, $p = .009$, $\eta^2 = 0.24$).

3.4 | Increased SUVr values in the putamen

We found significant increased SUVr in the bilateral putamen (left putamen: peak voxel $[-33, -4, 1]$, $T_{(55)} = 6.42$, $P_{FWE} < 0.001$, $\eta^2 = 0.39$; right putamen: peak voxel $[36, -5, 3]$ $T_{(55)} = 6.65$, $P_{FWE} < 0.001$, $\eta^2 = 0.39$, Figure 2). Voxels with $T > 3.48$ were considered significant after small volume correction. The averaged SUVr of the bilateral substantia nigra was not significantly different between the two groups ($p = .84$). No significant correlations were found between the putamen SUVr and the clinical measurements (p values $>.14$).

3.5 | Decreased nigral-putamen FC

We found significant decreased FC between the substantia nigra and the anterior putamen (left peak voxel at $[-18, 18, -6]$, $T_{(55)} = -5.43$, $P_{FWE} < 0.001$, $\eta^2 = 0.36$; right peak voxel at $[24, 9, 12]$, $T_{(55)} = -4.42$, $P_{FWE} = 0.007$, $\eta^2 = 0.26$ Figure 3a,b). Voxels with $T < -3.79$ were considered significant after small volume correction. Post hoc Lilliefors tests (Lilliefors, 1967) demonstrated that the FC and iron deposition in the substantia nigra were normally distributed (p values >0.19). The FC value from the left peak voxel was further negatively correlated with HY-stage ($R = -0.35$, $p = .04$, $\eta^2 = 0.08$, Figure 3c). and iron deposition in the substantia nigra ($R = -0.29$, $p = .04$, $\eta^2 = 0.12$, group and SN-

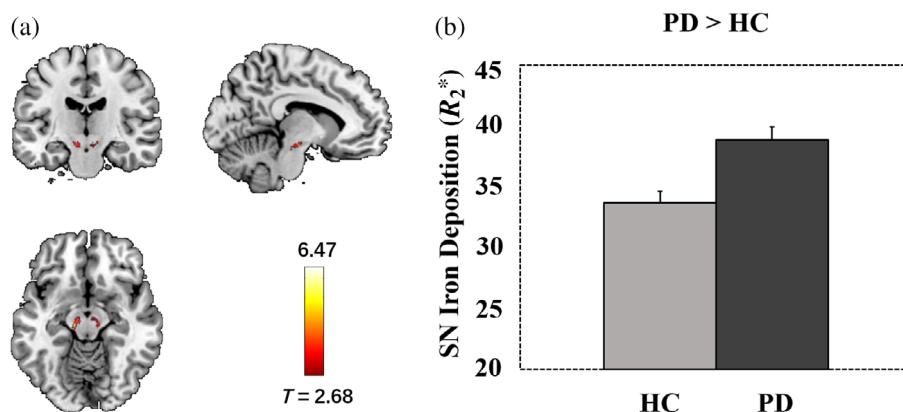


FIGURE 1 Increased SN iron deposition panel (a) shows the spatial distribution of increased iron deposition in the bilateral substantia nigra with a $p < .005$ uncorrected threshold. Please note that (a) was only for illustration purpose and we did not perform further statistical analyses. Panel (b) shows the bar plot of averaged iron deposition extracted from the bilateral substantia nigra ROI. There was an increased iron deposition in PD group ($p = .007$). Further statistical analyses as well as inference was based on the results showing in Figure 2b. Error bars represent standard error. Age and SN-GMV were controlled as covariates of non-interests

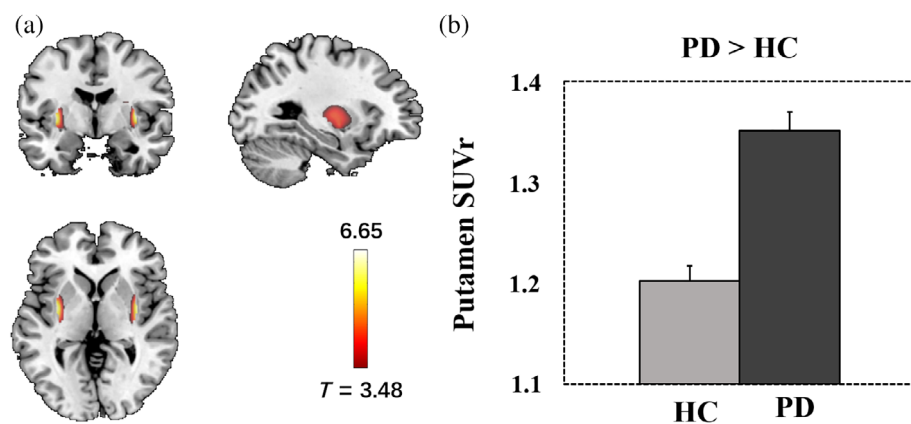


FIGURE 2 Increased putamen FDG uptake. Panel (a) shows the $p < .05$ corrected results of increased FDG uptake in the bilateral putamen. Results were masked with bilateral putamen from the AAL template. Age was controlled as covariates of non-interests. Panel (b) shows the bar plot of averaged putamen SUVr extracted from the clusters shown in panel (a). Error bars represent standard errors

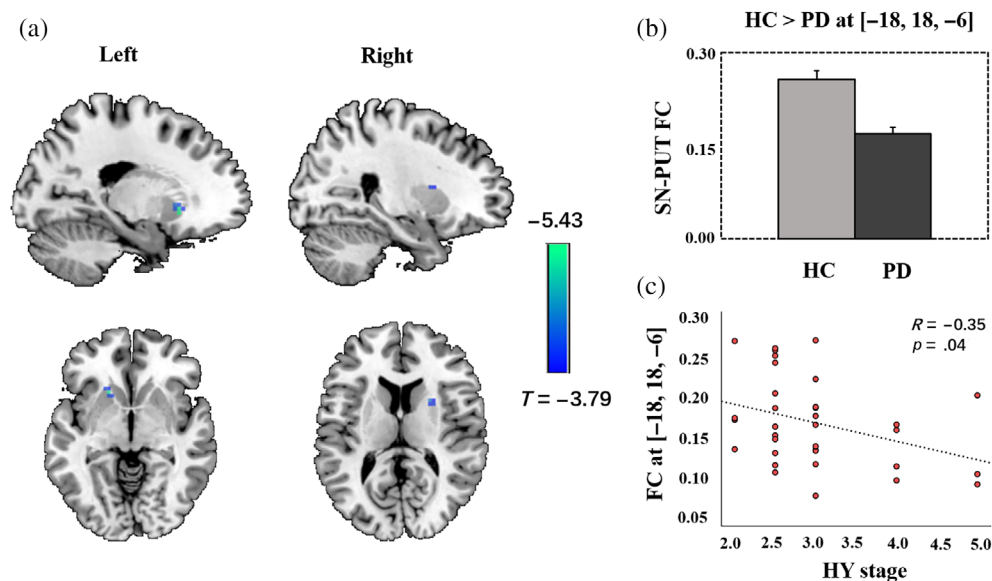


FIGURE 3 Decreased SN-PUT FC. Panel (a) shows $p < .05$ corrected results of decreased FC between the substantia nigra and the putamen (14 voxels, masked by bilateral putamen of the AAL template). Age and FD were controlled as covariates of non-interests. Panel (b) shows the post hoc bar plots of the peak voxel in the putamen (error bars are standard errors). Panel (c) shows the regression plot between the peak FC $[-18, 18, -6]$ and the HY-stage ($R = -0.35$, $p = .04$)

GMV as covariates of non-interests, Figure 4). No significant correlations were found between the nigral-putamen FC and UPDRS III as well as disease duration (p values $>.91$). We in addition replicated our FC finding using more stringent head motion correction approach (scrubbing) (Power et al., 2012) and different mask for the definition of substantia nigra (AAL3) (Rolls et al., 2020). As a result, we found decreased FC between the substantia nigra and putamen using the scrubbing (left peak $P_{FWE} = 0.02$, Figure S2A) or the substantia nigra mask from AAL3 (left peak $P_{FWE} = 0.04$, right peak $P_{FWE} = 0.008$, Figure S2B). These results demonstrated that the nigral-putamen FC finding was robust against different choice of head motion correction approach and substantia nigra ROI definition.

3.6 | Nigral iron deposition and nigral-putamen connectivity jointly modulate putamen glucose metabolism

Neither the nigral-putamen FC ($p = .70$) nor nigral iron deposition ($p = .93$) alone showed significant association with the putamen

SUVr value. However, there was a significant interaction effect of $Iron_{(SN)} \times FC_{(SN-PUT)}$ to putamen SUVr value ($F_{(1,46)} = 8.97$, $p = .004$, $\eta^2 = 0.16$, Figure 5), indicating that the iron deposition in the substantia nigra and nigral-putamen FC can jointly modulate putamen FDG-uptake.

Considering that there was no spatial overlap between the voxels showing increased FDG-uptake and decreased nigral-putamen FC after small volume correction, we further extracted the mean FC value from the voxels showing increased FDG-uptake within the bilateral putamen with less stringent thresholds ($p < .005$ uncorrected and $p < .05$ uncorrected). The FC values extracted using these two thresholds were not significantly different between the two groups ($p = .24$ and $.61$, respectively). We still found significant $Iron_{(SN)} \times FC_{(SN-PUT)}$ interaction effect on FDG-uptake in the posterior putamen (putamen masked with $p < .005$ uncorrected cluster: $F_{(1,46)} = 4.48$, $p = .04$, $\eta^2 = 0.09$; $p < .05$ uncorrected cluster: $F_{(1,46)} = 4.06$, $p = .049$, $\eta^2 = 0.08$). In addition, since we recruited moderate to severe PD patients, to further exclude the effect of disease severity on the $Iron_{(SN)} \times FC_{(SN-PUT)}$ interaction effect on putamen FDG-uptake, we conducted the same analysis in PD patients while controlling the

HY-stage as an additional covariate. Result indicated that the interaction effect was significant ($F_{[1,21]} = 8.62, p = .008$).

4 | DISCUSSION

In the current cross-sectional study, we detected increased R_2^* value in the substantia nigra, increased FDG-uptake in the putamen and decreased nigrostriatal FC distributed between the bilateral substantia nigra and the anterior putamen in the PD group compared to the healthy controls. The impaired FC was further correlated negatively

with HY-stage and iron deposition in the substantia nigra. By applying a general linear model that contains the interaction term of nigral iron deposition and nigral-putamen FC, a significant joint effect of the two features on the putamen FDG-uptake was detected. In the following paragraphs, we discuss our findings in detail.

4.1 | Nigral iron deposition, putamen FDG-uptake, and the nigral-putamen FC

We acquired simultaneous PET/MRI data which highly benefits better and more accurate function-metabolism coupling. As a result, we found increased iron deposition in the substantia nigra, increased FDG-uptake in the putamen and decreased nigral-putamen FC as replications of previous studies. First, in line with the existing literature (Graham et al., 2000; Langley et al., 2019; Liu et al., 2017; Zhang et al., 2010), we observed a significant increase of iron content in the bilateral substantia nigra in PD group which was recognized as a pathological hallmark in PD as revealed by post-mortem studies (Dexter et al., 1989; Riederer et al., 1989). Such findings can be reliably replicated by in vivo R_2^* (Langley et al., 2019) and QSM (Li et al., 2018) imaging technique. We then detected a significant decreased FC between the bilateral substantia nigra and the putamen in the patients with PD as an estimation of the impaired nigrostriatal pathway. The reduced FC finding in patients with PD was not only an independent replication of previous resting state fMRI (Hacker et al., 2012; Manza et al., 2016) and diffusion tractographic studies (Tan et al., 2015; Theisen et al., 2017), but also highly in line with the well-established nigrostriatal circuit model in PD (Dauer & Przedborski, 2003; McGregor & Nelson, 2019; Wichmann & DeLong, 2003).

Increased iron deposition in PD may indicate α -synuclein aggregation through iron-induced oxidative stress that associates with cellular deleterious in the substantia nigra (Guan et al., 2019; Sian-Hülsmann

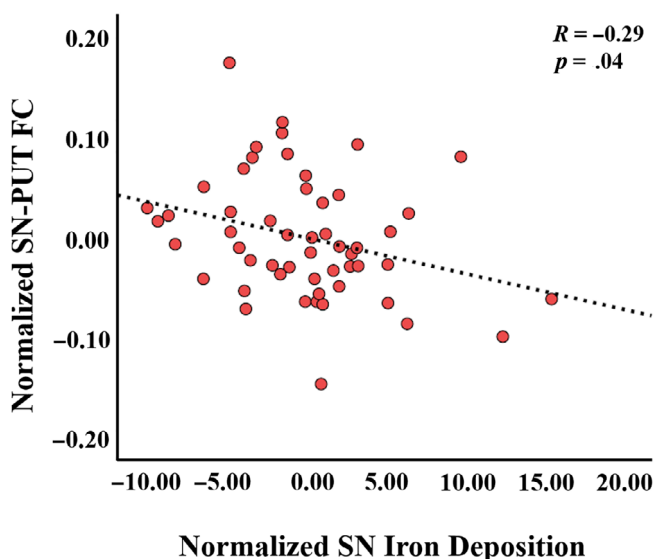
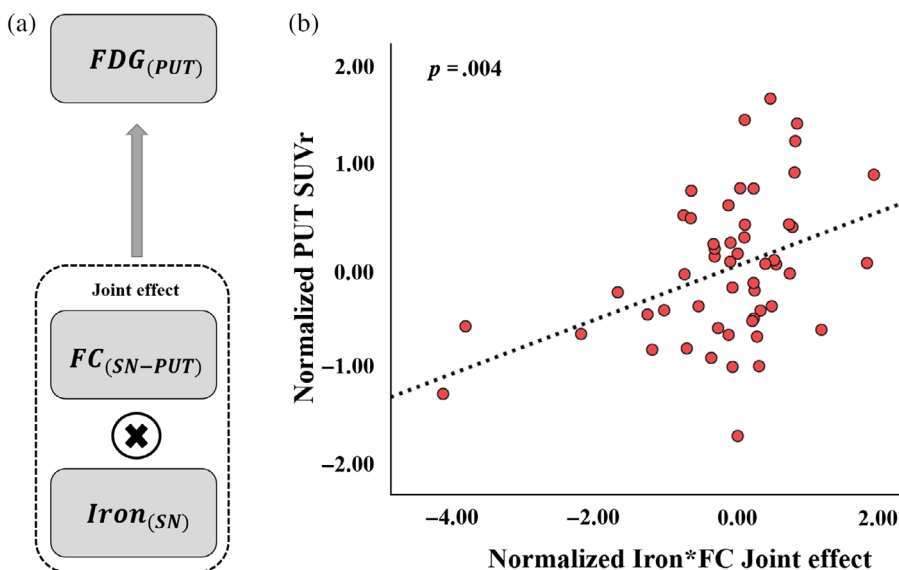


FIGURE 4 Association between SN-PUT connectivity and SN iron deposition. Figure shows the partial regression plot of iron deposition in the substantia nigra and peak FC $[-18, 18, -6]$ ($R = -0.29, p = .04$, group and SN-GMV as covariates of non-interests)

FIGURE 5 SN iron deposition and SN-PUT connectivity jointly modulate putamen FDG-uptake. Figure illustrates the significant interaction effect of nigral iron deposition and nigral-putamen connectivity on FDG-uptake in the putamen ($p = .004$). Panel (a) displays the concept chart-flow of the joint modulation effect. Panel (b) shows the partial regression plot of putamen FDG-uptake and Iron*FC joint effect from the general linear model. Group and SN-GMV were controlled as covariates of non-interests



et al., 2011). In our data, we obtained significant negative correlation between the decreased nigral-putamen FC and the HY-stage as well as iron deposition. Thus, we speculated that there was a connection between the toxic accumulation of iron in the substantia nigra and the impairment of the nigrostriatal pathway: the more impaired the pathway was, the more severe the patient was.

In parallel with the abundant existing ^{18}F -FDG PET studies (Albrecht et al., 2019; Eidelberg et al., 1994; Ruppert et al., 2020), we as well detected increased FDG-uptake in the putamen. The increased FDG-uptake was located mainly in the posterior putamen. While the reduction of FC was located in the anterior putamen. The location showing decreased nigral-putamen FC overlapped well with the location of decreased putamen resting state activity as shown in a multicenter meta-analysis study (Jia et al., 2021). In addition, by using dopamine cell implantation surgery, Ma and colleagues (Ma et al., 2010) have shown that the baseline ^{18}F -DOPA uptake in the dorsal anterior putamen, which locates close to the cluster of our FC finding, can predict UPDRS improvement. These studies demonstrated that the reduced FC may be associated more with dopaminergic degeneration.

4.2 | Nigral iron deposition and FC jointly modulate putamen glucose metabolism

Of note, the increased FDG-uptake in the putamen was neither correlated with nigral-putamen FC nor with iron deposition in the substantia nigra. Instead, result from the GLM analysis showed a significant iron deposition-by-nigral-putamen connectivity interaction effect on the putamen glucose metabolism, indicating that iron deposition in the substantia nigra and connectivity representing the nigrostriatal pathway can jointly modulate glucose metabolism of the putamen during resting state. As mentioned earlier, the location of the cluster exhibiting increased FDG-uptake in the putamen did not overlap with that showing reduced FC, we then replicated the joint modulation effect using the FC from the posterior putamen that showed increased FDG-uptake. We still found a significant iron deposition-by-nigral-putamen connectivity interaction effect on the putamen FDG-uptake, demonstrating that the significant joint effect was not highly influenced by the spatial distribution of the FC in the putamen. Although direct evidence was insufficient, we speculated from our finding that the joint modulation effect may explain the insufficient dopaminergic inhibitory input to the putamen (Eidelberg et al., 1994). Future studies with dopaminergic biomarkers are needed for clarification of such interpretation.

The current study may highlight the pathological role of the iron deposition in the substantia nigra, as it not only reflected the severity of the disease, but also explained the abnormal putamen metabolism together with nigra-putamen FC. From this perspective, a comprehensive neuroimaging examination of the substantia nigra may largely benefit clinical diagnose and treatment of PD.

4.3 | Limitations

First, we recruited moderate to severe patients with PD which restricted us to generate the current findings to mild patients. Second, we acknowledge that the recruitment and medication application of our patients is a major limitation to the current as well as other Parkinson' disease studies. The standard 12-h washout period may not be sufficient enough especially for the severe patients.

5 | CONCLUSIONS

In conclusion, we found significantly increased iron deposition in the substantia nigra and FDG-uptake in the putamen and decreased FC between the substantia nigra and putamen in patients with PD compared to the healthy controls. The nigral iron deposition and FC can jointly modulate putamen glucose metabolism, highlighting the utility of simultaneous PET/MRI to the understanding of in vivo neuropathological mechanism of PD.

ACKNOWLEDGMENT

We would like to thank Dr. Yongquan Ye, Dr. Yufeng Zang, and Dr. Tao Wu for their valuable suggestions regarding methodological considerations as well as results discussion.

CONFLICT OF INTEREST

No conflict of interests is declared by the authors.

AUTHOR CONTRIBUTIONS

Zhenxiang Zang: drafting the manuscript, study concept and design, analysis and interpretation of data, statistical analysis. **Tianbin Song:** manuscript revision, data acquisition. **Jiping Li:** data acquisition, clinical assessment, critical review. **Shaozhen Yan:** manuscript revision and critical review. **Binbin Nie:** data analysis. **Shanshan Mei:** data acquisition. **Jie Ma:** data acquisition. **Yu Yang:** data acquisition. **Baoci Shan:** manuscript revision and critical review. **Yuqing Zhang:** data acquisition, manuscript revision and critical review. **Jie Lu:** study concept, manuscript revision and critical review.

DATA AVAILABILITY STATEMENT

Data and materials are available under reasonable requests.

ORCID

Zhenxiang Zang  <https://orcid.org/0000-0002-6865-054X>

Shaozhen Yan  <https://orcid.org/0000-0002-0315-7930>

Baoci Shan  <https://orcid.org/0000-0001-7417-5063>

Jie Lu  <https://orcid.org/0000-0003-0425-3921>

REFERENCES

- Albrecht, F., Ballarini, T., Neumann, J., & Schroeter, M. L. (2019). FDG-PET hypometabolism is more sensitive than MRI atrophy in Parkinson's disease: A whole-brain multimodal imaging meta-analysis. *NeuroImage: Clinical*, 21, 101594. <https://doi.org/10.1016/j.nicl.2018.11.004>

- Bassett, D. S., Yang, M., Wymbs, N. F., & Grafton, S. T. (2015). Learning-induced autonomy of sensorimotor systems. *Nature Neuroscience*, 18(5), 744–751. <https://doi.org/10.1038/nn.3993>
- Braun, U., Schäfer, A., Bassett, D. S., Rausch, F., Schweiger, J. I., Bilek, E., Erk, S., Romanczuk-Seiferth, N., Grimm, O., Geiger, L. S., Haddad, L., Otto, K., Mohnke, S., Heinz, A., Zink, M., Walter, H., Schwarz, E., Meyer-Lindenberg, A., & Tost, H. (2016). Dynamic brain network reconfiguration as a potential schizophrenia genetic risk mechanism modulated by NMDA receptor function. *Proceedings of the National Academy of Sciences*, 113(44), 12568–12573. <https://doi.org/10.1073/pnas.1608819113>
- Chu, Y., Muller, S., Tavares, A., Barret, O., Alagille, D., Seibyl, J., Tamagnan, G., Marek, K., Luk, K. C., Trojanowski, J. Q., Lee, V. M. Y., & Kordower, J. H. (2019). Intrastriatal alpha-synuclein fibrils in monkeys: Spreading, imaging and neuropathological changes. *Brain*, 142(11), 3565–3579. <https://doi.org/10.1093/brain/awz296>
- Dauer, W., & Przedborski, S. (2003). Parkinson's disease: Mechanisms and models. *Neuron*, 39(6), 889–909. [https://doi.org/10.1016/s0896-6273\(03\)00568-3](https://doi.org/10.1016/s0896-6273(03)00568-3)
- DeLong, M. R. (1990). Primate models of movement disorders of basal ganglia origin. *Trends in Neurosciences*, 13(7), 281–285. [https://doi.org/10.1016/0166-2236\(90\)90110-v](https://doi.org/10.1016/0166-2236(90)90110-v)
- Dexter, D. T., Wells, F. R., Lees, A. J., Agid, F., Agid, Y., Jenner, P., & Marsden, C. D. (1989). Increased nigral iron content and alterations in other metal ions occurring in brain in Parkinson's disease. *Journal of Neurochemistry*, 52(6), 1830–1836. <https://doi.org/10.1111/j.1471-4159.1989.tb07264.x>
- Eidelberg, D., Moeller, J. R., Dhawan, V., Spetsieris, P., Takikawa, S., Ishikawa, T., Chaly, T., Robeson, W., Margouleff, D., Przedborski, S., & Fahh, S. (1994). The metabolic topography of parkinsonism. *Journal of Cerebral Blood Flow and Metabolism*, 14(5), 783–801. <https://doi.org/10.1038/jcbfm.1994.99>
- Graham, J. M., Paley, M. N., Grünewald, R. A., Hoggard, N., & Griffiths, P. D. (2000). Brain iron deposition in Parkinson's disease imaged using the PRIME magnetic resonance sequence. *Brain*, 123(Pt 12), 2423–2431. <https://doi.org/10.1093/brain/123.12.2423>
- Guan, X., Zhang, Y., Wei, H., Guo, T., Zeng, Q., Zhou, C., Wang, J., Gao, T., Xuan, M., Gu, Q., Xu, X., Huang, P., Pu, J., Zhang, B., Liu, C., & Zhang, M. (2019). Iron-related nigral degeneration influences functional topology mediated by striatal dysfunction in Parkinson's disease. *Neurobiology of Aging*, 75, 83–97. <https://doi.org/10.1016/j.neurobiolaging.2018.11.013>
- Hacker, C. D., Perlmutter, J. S., Criswell, S. R., Ances, B. M., & Snyder, A. Z. (2012). Resting state functional connectivity of the striatum in Parkinson's disease. *Brain*, 135(Pt 12), 3699–3711. <https://doi.org/10.1093/brain/awz281>
- Iravani, M. M., Syed, E., Jackson, M. J., Johnston, L. C., Smith, L. A., & Jenner, P. (2005). A modified MPTP treatment regime produces reproducible partial nigrostriatal lesions in common marmosets. *The European Journal of Neuroscience*, 21(4), 841–854. <https://doi.org/10.1111/j.1460-9568.2005.03915.x>
- Jeon, B. S., Jackson-Lewis, V., & Burke, R. E. (1995). 6-Hydroxydopamine lesion of the rat substantia nigra: Time course and morphology of cell death. *Neurodegeneration*, 4(2), 131–137. <https://doi.org/10.1006/neur.1995.0016>
- Jia, X. Z., Zhao, N., Dong, H. M., Sun, J. W., Barton, M., Burciu, R., Carrière, N., Cerasa, A., Chen, B. Y., Chen, J., Coombes, S., Defebvre, L., Delmaire, C., Dujardin, K., Esposito, F., Fan, G. G., Di Nardo, F., Feng, Y. X., Fling, B. W., ... Zang, Y. F. (2021). Small P values may not yield robust findings: An example using REST-meta-PD. *Science Bulletin*, 66, 2148–2152. <https://doi.org/10.1016/j.scib.2021.06.007>
- Langley, J., He, N., Huddleston, D. E., Chen, S., Yan, F., Crosson, B., Factor, S., & Hu, X. (2019). Reproducible detection of nigral iron deposition in 2 Parkinson's disease cohorts. *Movement Disorders*, 34(3), 416–419. <https://doi.org/10.1002/mds.27608>
- Lee, J. H., Han, Y. H., Kang, B. M., Mun, C. W., Lee, S. J., & Baik, S. K. (2013). Quantitative assessment of subcortical atrophy and iron content in progressive supranuclear palsy and parkinsonian variant of multiple system atrophy. *Journal of Neurology*, 260(8), 2094–2101. <https://doi.org/10.1007/s00415-013-6951-x>
- Li, D. T. H., Hui, E. S., Chan, Q., Yao, N., Chua, S. E., McAlonan, G. M., Pang, S. Y. Y., Ho, S. L., & Mak, H. K. F. (2018). Quantitative susceptibility mapping as an indicator of subcortical and limbic iron abnormality in Parkinson's disease with dementia. *NeuroImage: Clinical*, 20, 365–373. <https://doi.org/10.1016/j.nicl.2018.07.028>
- Lilliefors, H. W. (1967). On the Kolmogorov–Smirnov test for normality with mean and variance unknown. *Journal of the American Statistical Association*, 62(318), 399–402. <https://doi.org/10.2307/2283970>
- Liu, Z., Shen, H. C., Lian, T. H., Mao, L., Tang, S. X., Sun, L., Huang, X. Y., Guo, P., Cao, C. J., Yu, S. Y., Zuo, L. J., Wang, X. M., Chen, S. D., Chan, P., & Zhang, W. (2017). Iron deposition in substantia nigra: Abnormal iron metabolism, neuroinflammatory mechanism and clinical relevance. *Scientific Reports*, 7(1), 14973. <https://doi.org/10.1038/s41598-017-14721-1>
- Ma, Y., Tang, C., Chaly, T., Greene, P., Breeze, R., Fahh, S., Freed, C., Dhawan, V., & Eidelberg, D. (2010). Dopamine cell implantation in Parkinson's disease: Long-term clinical and (18)F-FDOPA PET outcomes. *Journal of Nuclear Medicine*, 51(1), 7–15. <https://doi.org/10.2967/jnumed.109.066811>
- Maiti, P., Manna, J., & Dunbar, G. L. (2017). Current understanding of the molecular mechanisms in Parkinson's disease: Targets for potential treatments. *Translational Neurodegeneration*, 6(1), 28. <https://doi.org/10.1186/s40035-017-0099-z>
- Manza, P., Zhang, S., Li, C. S., & Leung, H. C. (2016). Resting-state functional connectivity of the striatum in early-stage Parkinson's disease: Cognitive decline and motor symptomatology. *Human Brain Mapping*, 37(2), 648–662. <https://doi.org/10.1002/hbm.23056>
- McGregor, M. M., & Nelson, A. B. (2019). Circuit mechanisms of Parkinson's disease. *Neuron*, 101(6), 1042–1056. <https://doi.org/10.1016/j.neuron.2019.03.004>
- Meyer, P. T., Frings, L., Rücker, G., & Hellwig, S. (2017). (18)F-FDG PET in parkinsonism: Differential diagnosis and evaluation of cognitive impairment. *Journal of Nuclear Medicine*, 58(12), 1888–1898. <https://doi.org/10.2967/jnumed.116.186403>
- Nie, B., Liang, S., Jiang, X., Duan, S., Huang, Q., Zhang, T., Li, P., Liu, H., & Shan, B. (2018). An automatic method for generating an unbiased intensity normalizing factor in positron emission tomography image analysis after stroke. *Neuroscience Bulletin*, 34(5), 833–841. <https://doi.org/10.1007/s12264-018-0240-8>
- Ostrerova-Golts, N., Petrucelli, L., Hardy, J., Lee, J. M., Farer, M., & Wolozin, B. (2000). The A53T alpha-synuclein mutation increases iron-dependent aggregation and toxicity. *The Journal of Neuroscience*, 20(16), 6048–6054. <https://doi.org/10.1523/jneurosci.20-16-06048.2000>
- Pauli, W. M., Nili, A. N., & Tyszka, J. M. (2018). A high-resolution probabilistic in vivo atlas of human subcortical brain nuclei. *Scientific Data*, 5, 180063. <https://doi.org/10.1038/sdata.2018.63>
- Porras, G., Li, Q., & Bezard, E. (2012). Modeling Parkinson's disease in primates: The MPTP model. *Cold Spring Harbor Perspectives in Medicine*, 2(3), a009308. <https://doi.org/10.1101/cshperspect.a009308>
- Postuma, R. B., Berg, D., Stern, M., Poewe, W., Olanow, C. W., Oertel, W., Obeso, J., Marek, K., Litvan, I., Lang, A. E., Halliday, G., Goetz, G. C., Gasser, T., Dubois, B., Chan, P., Bloem, B. R., Adler, C. H., & Deuschl, G. (2015). MDS clinical diagnostic criteria for Parkinson's disease. *Movement Disorders*, 30(12), 1591–1601. <https://doi.org/10.1002/mds.26424>
- Postuma, R. B., Poewe, W., Litvan, I., Lewis, S., Lang, A. E., Halliday, G., Goetz, C. G., Chan, P., Slow, E., Seppi, K., Schaffer, E., Rios-Romenets, S., Mi, T., Maetzler, C., Li, Y., Heim, B., Bledsoe, I. O., & Berg, D. (2018). Validation of the MDS clinical diagnostic criteria for Parkinson's

- disease. *Movement Disorders*, 33(10), 1601–1608. <https://doi.org/10.1002/mds.27362>
- Power, J. D., Barnes, K. A., Snyder, A. Z., Schlaggar, B. L., & Petersen, S. E. (2012). Spurious but systematic correlations in functional connectivity MRI networks arise from subject motion. *NeuroImage*, 59(3), 2142–2154. <https://doi.org/10.1016/j.neuroimage.2011.10.018>
- Rentsch, P., Stayte, S., Morris, G. P., & Vissel, B. (2019). Time dependent degeneration of the nigrostriatal tract in mice with 6-OHDA lesioned medial forebrain bundle and the effect of activin A on L-Dopa induced dyskinesia. *BMC Neuroscience*, 20(1), 5. <https://doi.org/10.1186/s12868-019-0487-7>
- Riederer, P., Sofic, E., Rausch, W. D., Schmidt, B., Reynolds, G. P., Jellinger, K., & Youdim, M. B. (1989). Transition metals, ferritin, glutathione, and ascorbic acid in parkinsonian brains. *Journal of Neurochemistry*, 52(2), 515–520. <https://doi.org/10.1111/j.1471-4159.1989.tb09150.x>
- Rolls, E. T., Huang, C. C., Lin, C. P., Feng, J., & Joliot, M. (2020). Automated anatomical labelling atlas 3. *NeuroImage*, 206, 116189. <https://doi.org/10.1016/j.neuroimage.2019.116189>
- Ruppert, M. C., Greuel, A., Tahmasian, M., Schwartz, F., Stürmer, S., Maier, F., Hammes, J., Tittgemeyer, M., Timmermann, L., Van Eimeren, T., Drzezga, A., & Eggers, C. (2020). Network degeneration in Parkinson's disease: Multimodal imaging of nigro-striato-cortical dysfunction. *Brain*, 143(3), 944–959. <https://doi.org/10.1093/brain/awaa019>
- Salami, A., Avelar-Pereira, B., Garzón, B., Sitnikov, R., & Kalpouzos, G. (2018). Functional coherence of striatal resting-state networks is modulated by striatal iron content. *NeuroImage*, 183, 495–503. <https://doi.org/10.1016/j.neuroimage.2018.08.036>
- Schindlbeck, K. A., & Eidelberg, D. (2018). Network imaging biomarkers: Insights and clinical applications in Parkinson's disease. *Lancet Neurology*, 17(7), 629–640. [https://doi.org/10.1016/s1474-4422\(18\)30169-8](https://doi.org/10.1016/s1474-4422(18)30169-8)
- Sian-Hülsmann, J., Mandel, S., Youdim, M. B., & Riederer, P. (2011). The relevance of iron in the pathogenesis of Parkinson's disease. *Journal of Neurochemistry*, 118(6), 939–957. <https://doi.org/10.1111/j.1471-4159.2010.07132.x>
- Tan, W. Q., Yeoh, C. S., Rumpel, H., Nadkarni, N., Lye, W. K., Tan, E. K., & Chan, L. L. (2015). Deterministic tractography of the nigrostriatal-nigropallidal pathway in Parkinson's disease. *Scientific Reports*, 5, 17283. <https://doi.org/10.1038/srep17283>
- Theisen, F., Leda, R., Pozorski, V., Oh, J. M., Adluru, N., Wong, R., Okonkwo, O., Dean, D. C., 3rd, Bendlin, B. B., Johnson, S. C., Alexander, A. L., & Gallagher, C. L. (2017). Evaluation of striatonigral connectivity using probabilistic tractography in Parkinson's disease. *NeuroImage: Clinical*, 16, 557–563. <https://doi.org/10.1016/j.nicl.2017.09.009>
- Ward, R. J., Zucca, F. A., Duyn, J. H., Crichton, R. R., & Zecca, L. (2014). The role of iron in brain ageing and neurodegenerative disorders. *Lancet Neurology*, 13(10), 1045–1060. [https://doi.org/10.1016/s1474-4422\(14\)70117-6](https://doi.org/10.1016/s1474-4422(14)70117-6)
- Wichmann, T., & DeLong, M. R. (2003). Pathophysiology of Parkinson's disease: The MPTP primate model of the human disorder. *Annals of the New York Academy of Sciences*, 991, 199–213. <https://doi.org/10.1111/j.1749-6632.2003.tb07477.x>
- Wooten, G. F., & Collins, R. C. (1981). Metabolic effects of unilateral lesion of the substantia nigra. *The Journal of Neuroscience*, 1(3), 285–291. <https://doi.org/10.1523/jneurosci.01-03-00285.1981>
- Ye, Y., Lyu, J., Sun, W., Lan, L., Wang, L., Zhang, W., & Xu, H. (2021). A multi-dimensional integration (MDI) strategy for MR T(2) * mapping. *NMR in Biomedicine*, 34, e4529. <https://doi.org/10.1002/nbm.4529>
- Zang, Z., Geiger, L. S., Braun, U., Cao, H., Zangl, M., Schäfer, A., Moessnang, C., Ruf, M., Reis, J., Schweiger, J. I., Dixon, L., Moscicki, A., Schwarz, E., Meyer-Lindenberg, A., & Tost, H. (2018). Resting-state brain network features associated with short-term skill learning ability in humans and the influence of N-methyl-d-aspartate receptor antagonism. *Network Neuroscience*, 2(4), 464–480. https://doi.org/10.1162/netn_a_00045
- Zhang, J., Zhang, Y., Wang, J., Cai, P., Luo, C., Qian, Z., Dai, Y., & Feng, H. (2010). Characterizing iron deposition in Parkinson's disease using susceptibility-weighted imaging: An in vivo MR study. *Brain Research*, 1330, 124–130. <https://doi.org/10.1016/j.brainres.2010.03.036>

SUPPORTING INFORMATION

Additional supporting information may be found in the online version of the article at the publisher's website.

How to cite this article: Zang, Z., Song, T., Li, J., Yan, S., Nie, B., Mei, S., Ma, J., Yang, Y., Shan, B., Zhang, Y., & Lu, J. (2022). Modulation effect of substantia nigra iron deposition and functional connectivity on putamen glucose metabolism in Parkinson's disease. *Human Brain Mapping*, 43(12), 3735–3744. <https://doi.org/10.1002/hbm.25880>